

Electron-phonon beyond Fröhlich: dynamical quadrupoles in polar and covalent solids

Guillaume Brunin¹, Henrique Pereira Coutada Miranda¹, Matteo Giantomassi¹, Miquel Royo², Massimiliano Stengel^{2,3}, Matthieu J. Verstraete^{4,5}, Xavier Gonze^{1,6}, Gian-Marco Rignanese¹, and Geoffroy Hautier¹

¹*UCLouvain, Institute of Condensed Matter and Nanosciences (IMCN),*

Chemin des Étoiles 8, B-1348 Louvain-la-Neuve, Belgium

²*Institut de Ciència de Materials de Barcelona (ICMAB-CSIC), Campus UAB, 08193 Bellaterra, Spain*

³*ICREA-Institució Catalana de Recerca i Estudis Avançats, 08010 Barcelona, Spain*

⁴*NanoMat/Q-Mat/CESAM, Université de Liège (B5), B-4000 Liège, Belgium*

⁵*Catalan Institute of Nanoscience and Nanotechnology (ICN2), Campus UAB, 08193 Bellaterra, Spain and*

⁶*Skolkovo Institute of Science and Technology, Moscow, Russia*

(Dated: February 4, 2020)

We include quadrupolar fields beyond the Fröhlich interaction in the first-principles electron-phonon vertex of semiconductors, and demonstrate their importance in calculations of carrier mobilities. Without such quadrupolar corrections, jump discontinuities for $\mathbf{q} \rightarrow \mathbf{0}$ remain in the short-range components. They lead to Gibbs oscillations in the interpolant, and affect the accuracy of the physical results. We apply our formalism to Si (non-polar), GaAs and GaP (polar). Electron mobilities converge much faster with the initial *ab initio* \mathbf{q} -mesh when dynamical quadrupoles are properly included.

The electron-phonon (e-ph) interaction plays a key role in the description of a variety of physical phenomena such as electronic transport, phonon-assisted light absorption, and phonon-mediated superconductivity [1]. In state-of-the-art *ab initio* methods, the e-ph coupling is described within density functional theory (DFT) by expanding the Kohn-Sham (KS) effective potential [2] in the nuclear displacements, and the vibrational properties are obtained with density-functional perturbation theory (DFPT) [3, 4]. This DFPT-based computational scheme enables the calculation of screened e-ph matrix elements on a microscopic level with *ab initio* quality [1]. However, e-ph related properties require an accurate description of the coupling on very dense grids in the full Brillouin zone (BZ) thus rendering direct *ab initio* e-ph computations in real materials impracticable.

For this reason, different methods have been proposed to interpolate the e-ph matrix elements from initial coarse grids to dense ones. These approaches rely on localized basis sets such as maximally-localized Wannier functions [5–7] or atomic orbitals [8] to perform a Fourier interpolation of the e-ph vertex. Other works suggested to employ Fourier transforms to interpolate the local part of the scattering potentials and then use Bloch states to obtain the e-ph matrix elements on dense grids [9, 10].

Despite formal differences in the treatment of the electron wavefunctions, all these approaches rely on the spatial localization of the scattering potentials for obtaining a reliable interpolation in the phonon wavevector \mathbf{q} . In Fourier-based interpolation schemes, indeed, the signal in real space is assumed to be negligibly small beyond a certain distance so that a faithful interpolation in \mathbf{q} -space can be obtained with a relatively coarse sampling of the BZ. In semiconductors and insulators, however, the incomplete screening of the external potential generated by the atomic displacements leads to long-range

(LR) interactions. In polar materials, these interactions manifest in the long-wavelength limit ($\mathbf{q} \rightarrow \mathbf{0}$) by the LO-TO splitting of the optical frequencies [11] and the Fröhlich divergence of the e-ph matrix elements [12] that are not amenable to Fourier interpolation due to their non-analytic behavior. The treatment of the LR dipole-dipole interaction in the Fourier interpolation of the dynamical matrix was developed in the early days of DFPT and the methodology is well documented [3, 4]. Only recently, it was shown how to generalize the Fröhlich contribution to e-ph matrix elements to anisotropic materials and how to integrate it with Wannier-based interpolation schemes [6, 13].

In this letter, we go beyond these contributions by demonstrating the importance of the next-to-leading order terms derived by Vogl [14]. We develop an approach to interpolate the short-range (SR) part of the scattering potentials on dense \mathbf{q} -grids while the LR contributions are expressed in terms of the high-frequency dielectric tensor, Born effective charges (dipole potential), dynamical quadrupoles computed from first principles using the theory of spatial dispersion [15, 16] (quadrupole potential) and the response to a homogeneous static electric field (local-field potential, also quadrupolar) already available in many DFPT implementations [3, 4]. In non-polar materials, the quadrupolar fields represent the leading contribution to the LR part, that should therefore be taken into account for accurate interpolations. In polar semiconductors, quadrupole terms are in principle small when compared to the divergent Fröhlich interaction but their non-analytical behavior for $\mathbf{q} \rightarrow \mathbf{0}$ implies a LR behavior in real space that will spoil any Fourier-based interpolation technique if not handled properly. Our formalism generalizes the previous approaches [6, 13] by including contributions that are crucial to achieve reliable and accurate e-ph calculations in semiconductors. We

demonstrate the importance of the quadrupole corrections by analyzing the convergence rate of electron mobilities in Si and GaAs. Additional results for GaP can be found in the Supplemental Material [17]. Without quadrupoles, carrier mobilities are plagued by an exceedingly slow convergence with respect to the initial *ab initio* \mathbf{q} -mesh. Stable results can be achieved with reasonable \mathbf{q} -meshes only when quadrupolar fields are separated from the SR part before the interpolation. Further details concerning our implementation including additional convergence studies and results for the electron mobility of GaP are given in our accompanying manuscript [18].

The key ingredients in e-ph computations are the coupling matrix elements $g_{mn\nu}(\mathbf{k}, \mathbf{q}) = \langle \psi_{m\mathbf{k}+\mathbf{q}} | \Delta_{\mathbf{q}\nu} V | \psi_{n\mathbf{k}} \rangle$ with $\psi_{n\mathbf{k}}$ the $n\mathbf{k}$ Bloch state and $\Delta_{\mathbf{q}\nu} V$ the first-order variation of the KS potential V due to a phonon mode of wavevector \mathbf{q} and branch index ν [1]. The scattering potential is defined as

$$\Delta_{\mathbf{q}\nu} V = e^{i\mathbf{q}\cdot\mathbf{r}} \frac{1}{\sqrt{2\omega_{\mathbf{q}\nu}}} \sum_{\kappa\alpha} \frac{e_{\kappa\alpha,\nu}(\mathbf{q})}{\sqrt{M_\kappa}} V_{\kappa\alpha,\mathbf{q}}(\mathbf{r}) \quad (1)$$

with $\omega_{\mathbf{q}\nu}$ the phonon frequency and $e_{\kappa\alpha,\nu}(\mathbf{q})$ the α -th Cartesian component of the phonon eigenvector for the atom κ of mass M_κ in the unit cell. $V_{\kappa\alpha,\mathbf{q}}(\mathbf{r})$ is the lattice-periodic scattering potential computed with DFPT [19]. Following the same approach as Verdi *et al.* [13], the e-ph scattering potential is separated into SR (\mathcal{S}) and LR (\mathcal{L}) contributions:

$$V_{\kappa\alpha,\mathbf{q}}(\mathbf{r}) = V_{\kappa\alpha,\mathbf{q}}^{\mathcal{S}}(\mathbf{r}) + V_{\kappa\alpha,\mathbf{q}}^{\mathcal{L}}(\mathbf{r}). \quad (2)$$

$$V_{\kappa\alpha,\mathbf{q}}^{\mathcal{L}}(\mathbf{r}) = \frac{4\pi}{\Omega} \sum_{\mathbf{G}\neq-\mathbf{q}} \frac{i(q_\beta + G_\beta)Z_{\kappa\alpha,\beta}^* - (q_\beta + G_\beta)(q_\gamma + G_\gamma)(Z_{\kappa\alpha,\beta}^* \mathcal{Q} v^{\text{Hxc},\mathcal{E}_\gamma}(\mathbf{r}) - \frac{1}{2} \mathcal{Q}_{\kappa\alpha}^{\beta\gamma})}{(q_\delta + G_\delta)\epsilon_{\delta\delta'}^\infty(q_{\delta'} + G_{\delta'})} e^{i(q_\eta + G_\eta)(r_\eta - \tau_{\kappa\eta})}, \quad (4)$$

where $\mathbf{Q}_{\kappa\alpha}$ is the dynamical quadrupole tensor, \mathcal{Q} is the electronic charge in atomic units, that is, -1 , and $v^{\text{Hxc},\mathcal{E}_\gamma}$ is the change of the Hartree and exchange-correlation potential with respect to the electric field \mathcal{E} in Cartesian coordinates (see Ref. [18] for the derivation). In Eq. (4), the term related to $\mathbf{Q}_{\kappa\alpha}$ is non-zero even in non-polar semiconductors while the contribution associated to \mathcal{E} is present only in systems with non-zero Born effective charges.

In the polar systems that we investigated so far, we observed that $\mathbf{Q}_{\kappa\alpha}$ gives the most important contribution to Eq. (4) when compared to the \mathcal{E} term [17]. For instance, ignoring the \mathcal{E} term changes the electron mobility in GaAs by 0.1% and by 0.01% in GaP (see next

$V^{\mathcal{L}}$ is supposed to include all the LR components so that $V^{\mathcal{S}}$ is smooth in \mathbf{q} -space and therefore tractable with Fourier interpolation. In the interpolation algorithm, $V^{\mathcal{L}}$ is first subtracted from the DFPT potentials, then the Fourier interpolation is performed on the SR part only, finally $V^{\mathcal{L}}$ evaluated at the interpolated \mathbf{q} -point is added back [18]. In polar materials, the leading contribution to the LR part stems from the diverging Fröhlich-like potential [13]:

$$V_{\kappa\alpha,\mathbf{q}}^{\mathcal{L}(F)}(\mathbf{r}) = i \frac{4\pi}{\Omega} \sum_{\mathbf{G}\neq-\mathbf{q}} \frac{(q_\beta + G_\beta)Z_{\kappa\alpha,\beta}^* e^{i(q_\eta + G_\eta)(r_\eta - \tau_{\kappa\eta})}}{(q_\delta + G_\delta)\epsilon_{\delta\delta'}^\infty(q_{\delta'} + G_{\delta'})} \quad (3)$$

with Ω the unit cell volume, \mathbf{G} a reciprocal lattice vector, \mathbf{Z}_κ^* the Born effective charge tensor, ϵ^∞ the high-frequency dielectric tensor and τ_κ the position of the κ -th atom in the unit cell. The summation over repeated indices (β, η, δ and δ') is implied in Eq. (3) and in the following, unless the sum is explicitly written.

Most investigations so far have been focusing on the treatment of Eq. (3) because the (integrable) divergence for $\mathbf{q} \rightarrow \mathbf{0}$ is expected to give an important contribution to the BZ integrals. However, as discussed by Vogl [14] and rederived in a DFPT context in Ref. [18], a careful analysis of the asymptotic behavior of the scattering potential in the long-wavelength limit reveals the presence of additional non-analytical terms besides Eq. (3). These are finite for $\mathbf{q} \rightarrow \mathbf{0}$ but their non-analytic behavior (discontinuities) will affect the spatial decay of the scattering potentials even when the dipole interaction given by Eq. (3) is properly accounted for. Both dipole and quadrupole terms can be included in the LR potential using the generalized expression [18]:

paragraphs for more details about the mobility computations). Qualitatively, this behavior can be rationalized as follows. In the ionic limit, the potential change due to \mathcal{E} can be understood as a local linear potential created around each atom. Its average must be zero, but there will be regions of constant positive shift and zones of constant negative shift. If the orbitals are centered on each atom (so that the charge density is symmetric around it), the symmetry of the charge and the anti-symmetry of the potential give a vanishing contribution. In other words, after the Fröhlich divergence, the spatial decay of the scattering potentials is governed by the dynamical quadrupoles $\mathbf{Q}_{\kappa\alpha}$ at least as far as the materials considered here are concerned. Strictly speaking, it is not

possible to generalize this observation on the predominance of $\mathbf{Q}_{\kappa\alpha}$ to other non-polar systems although it is reasonable to expect that the same picture will be valid.

Note also that $\mathbf{Q}_{\kappa\alpha}$ introduces additional dipole-quadrupole and quadrupole-quadrupole terms at the level of the dynamical matrix [16] that are important to improve the accuracy of the interpolated phonon spectrum. Our calculations in Si, GaAs and GaP revealed that these extra terms in the Fourier interpolation of the dynamical matrix can accelerate the convergence of mobilities at the level of $\sim 1\%$, an effect that is smaller when compared to the error introduced by the Fourier interpolation of the e-ph potentials (discussed below) and yet larger than the correction due to the electric field. In the following, we will therefore focus on the contribution of $\mathbf{Q}_{\kappa\alpha}$ while the effects associated to the electric field, the dipole-quadrupole and the quadrupole-quadrupole interactions in the dynamical matrix are discussed in [17].

We begin by analyzing the effect of $\mathbf{Q}_{\kappa\alpha}$ on the interpolation of the scattering potentials and of the matrix elements. Then we discuss the convergence behavior of electron mobilities with respect to the *ab initio* \mathbf{q} -grid. The numerical values of $\mathbf{Q}_{\kappa\alpha}$ are computed using the recent implementation of Royo *et al.* [15] that has been integrated with the e-ph part of ABINIT [18, 20, 21].

In Figs. 1(a) and (b) we plot the average over the unit cell of the lattice-periodic part of the scattering potential,

$$\bar{V}_{\kappa\alpha,\mathbf{q}} = \frac{1}{\Omega} \int_{\Omega} d\mathbf{r} V_{\kappa\alpha,\mathbf{q}}(\mathbf{r}) e^{-i\mathbf{q}\cdot\mathbf{r}}, \quad (5)$$

for selected atomic perturbations in Si and GaAs, along a high-symmetry \mathbf{q} -path. The *exact* DFPT results (blue lines) are compared with those obtained with the models with (green) or without (red) quadrupole corrections of Eqs. (3) and (4) [22]. The other potentials, for all perturbations, are reported in the Supplemental Material [17]. In Si, the Born effective charges are zero and the imaginary part of the potential does not diverge for $\mathbf{q} \rightarrow \mathbf{0}$ (see dashed lines in Fig. 1(a)). In GaAs, the Fröhlich-like model in Eq. (3) correctly describes the divergence of the imaginary part of the potential close to Γ (see green dashed line in Fig. 1(b)). In both materials, however, the real part of the potential (solid lines) presents a jump discontinuity for $\mathbf{q} \rightarrow \mathbf{0}$. Note that the Fröhlich term alone does not capture this non-analyticity. On the contrary, if the quadrupole $\mathbf{Q}_{\kappa\alpha}$ contributions are included through Eq. (4), the LR model reproduces these jumps as shown by the solid green lines in Figs. 1(a) and (b). Figure 1(c) shows the real part of the average of the scattering potential in Si interpolated from a $9 \times 9 \times 9$ \mathbf{q} -point grid onto the same \mathbf{q} -path as in Fig. 1(a). If the $\mathbf{Q}_{\kappa\alpha}$ terms are not removed from the input DFPT potentials, the Fourier interpolation introduces unphysical sharp oscillations for small \mathbf{q} (see red line, FI). The correct behavior is properly reproduced only when $\mathbf{Q}_{\kappa\alpha}$

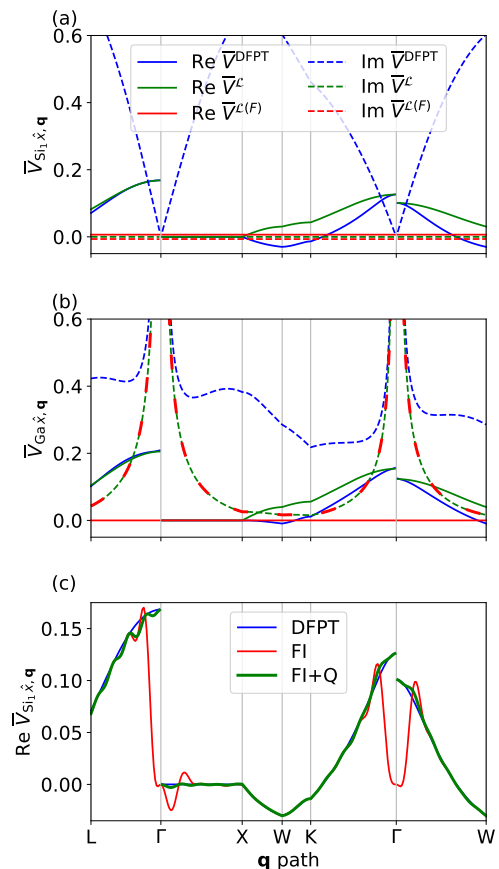


FIG. 1. Comparison between the average over the unit cell of the exact DFPT potentials (\bar{V}^{DFPT}) and the models of Eqs. (3) ($\bar{V}^{\mathcal{L}(F)}$) and (4) ($\bar{V}^{\mathcal{L}}$) in (a) Si and (b) GaAs. We consider the first reduced component \hat{x} of the DFPT potentials for (a) the Si and (b) the Ga atoms located at $(0,0,0)$. (c) Fourier interpolation (FI) of the real part of the potentials shown in (a) with (FI+Q) and without (FI) quadrupolar contribution. The potentials are given in Hartree/Bohr. The path has been sampled with 278 \mathbf{q} -points.

is included (see green line, FI+Q). Small oscillations are still appreciable around Γ when a $9 \times 9 \times 9$ \mathbf{q} -mesh is used but these deviations have a limited effect on the final electron mobilities.

It is worth stressing that these considerations hold for any approach employing Fourier-based interpolations. The discontinuity of the matrix elements at Γ and the discrepancy between the interpolant and the *exact* DFPT results in the region around Γ have already been noticed for Si and diamond [8]. The resulting error was considered harmless under the assumption that it is always possible to improve the accuracy of the Fourier interpolation by densifying the initial *ab initio* \mathbf{q} -mesh [8]. Unfortunately, this assumption does not hold in the presence of non-analytical behavior since, strictly speaking, an infinite number of Fourier components (*i.e.* an infinite number of real space lattice vectors \mathbf{R}) would be

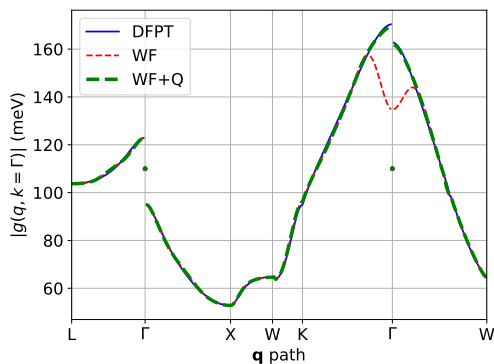


FIG. 2. E-ph matrix elements in Si computed with QE, and interpolated using Wannier functions with the standard EPW approach (WF) or including the quadrupolar corrections (WF+Q).

needed to represent the discontinuous signal. To confirm our hypothesis, we modified the EPW code [7] to include the $\mathbf{Q}_{\kappa\alpha}$ terms in the interpolation of the e-ph matrix elements in the Wannier representation in Si [23]. Figure 2 shows the e-ph matrix elements connecting the electron state at the valence band maximum at $\mathbf{k} = \Gamma$ to the other highest states of the valence band through the highest phonon mode at L as in Ref. [8]. The DFPT results (blue solid line) and the Wannier-interpolated results (red and green dashed lines) are compared in this figure. The interpolation of the matrix elements using the standard approach (*i.e.* without $\mathbf{Q}_{\kappa\alpha}$) leads to systematic errors in the region around the Γ point associated to electronic transitions with small momentum transfer. Including the dynamical quadrupoles in the model significantly improves the quality of the interpolant around the Γ point. Similar behaviour is also expected in e-ph calculations based on supercells and finite differences [10].

At this point, one question arises spontaneously: can we ignore such physical effects, and simply interpolate with an exceedingly dense grid around Γ ? To answer this question, we need to quantify the error introduced by these spurious oscillations in the final physical results. Because of intra-valley transitions, the region around Γ is one of the most important for the description of e-ph scattering processes [17, 18]. An accurate description in this region is crucial for reliable calculations of the phonon-induced electron linewidths,

$$\begin{aligned} \tau_{n\mathbf{k}}^{-1} = & 2\pi \sum_{m,\nu} \int_{\text{BZ}} \frac{d\mathbf{q}}{\Omega_{\text{BZ}}} |g_{m\nu}(\mathbf{k}, \mathbf{q})|^2 \\ & \times [(n_{\mathbf{q}\nu} + f_{m\mathbf{k}+\mathbf{q}})\delta(\varepsilon_{n\mathbf{k}} - \varepsilon_{m\mathbf{k}+\mathbf{q}} + \omega_{\mathbf{q}\nu}) \\ & + (n_{\mathbf{q}\nu} + 1 - f_{m\mathbf{k}+\mathbf{q}})\delta(\varepsilon_{n\mathbf{k}} - \varepsilon_{m\mathbf{k}+\mathbf{q}} - \omega_{\mathbf{q}\nu})], \end{aligned} \quad (6)$$

with Ω_{BZ} the BZ volume, $n_{\mathbf{q}\nu}$ and $f_{m\mathbf{k}+\mathbf{q}}$ the Bose-Einstein and Fermi-Dirac occupation functions and $\varepsilon_{n\mathbf{k}}$ the energy of the electronic state $n\mathbf{k}$. These linewidths represent the phonon-dependent ingredients needed to

compute carrier mobilities within the self-energy relaxation time approximation [1, 18, 24, 25]:

$$\mu_{e,\alpha\beta} = \frac{-1}{\Omega n_e} \sum_n \int \frac{d\mathbf{k}}{\Omega_{\text{BZ}}} v_{n\mathbf{k},\alpha} v_{n\mathbf{k},\beta} \tau_{n\mathbf{k}} \left. \frac{\partial f}{\partial \varepsilon} \right|_{\varepsilon_{n\mathbf{k}}}, \quad (7)$$

where $v_{n\mathbf{k},\alpha}$ is the α -th component of the velocity operator [18]. Figures 3(a) and (b) report the electron mobilities in Si and GaAs computed using plane waves with ABINIT as described in Ref. [18], as a function of the initial \mathbf{q} -grid. For each initial *ab initio* DFPT mesh, we interpolate the scattering potentials to obtain the lifetimes on \mathbf{k} - and \mathbf{q} -point meshes that are dense enough to reach convergence in the mobility within 5%. If the terms associated to the dynamical quadrupoles are included in the LR part of the potentials, a $9 \times 9 \times 9$ ($6 \times 6 \times 6$) \mathbf{q} -mesh is already sufficiently dense in Si (GaAs) for the correct interpolation of the potentials (green lines) whereas without $\mathbf{Q}_{\kappa\alpha}$ the convergence is much slower and not even reached with a $21 \times 21 \times 21$ \mathbf{q} -mesh (red lines). Using \mathbf{q} -grids typically reported in the literature ($8 \times 8 \times 8$) can therefore lead to significant errors at the level of the mobility. The error is around 10% in Si and goes up to 30% in GaAs where, due to the small effective mass, most of the scattering channels for electrons close to the band edge involve small momentum transfer. E-ph interpolations are usually performed starting from coarse \mathbf{q} -meshes because both the memory requirements and the computational cost of the interpolation quickly increase with the number of \mathbf{q} -points in the initial *ab initio* mesh hence it is not surprising that this behavior has been largely overlooked so far.

In conclusion, we have included quadrupolar fields beyond the Fröhlich interaction in the first-principles electron-phonon vertex of semiconductors. Their importance was demonstrated in calculations of mobilities. Accurate calculations of e-ph properties in semiconductors and insulators can be achieved with reasonably coarse *ab initio* \mathbf{q} -meshes provided that a careful treatment of the long-range interaction associated to dynamical quadrupoles is properly taken into account. We presented a fully *ab initio* formalism that employs $\mathbf{Q}_{\kappa\alpha}$ computed with DFPT to improve the description of the non-analytical behavior of the e-ph scattering potentials in the long-wavelength limit. Our approach improves state-of-the-art techniques that were mainly designed to cope with the Fröhlich-like interaction in polar materials. Since long-range macroscopic interactions play a key role in semiconductor physics, we believe that the quest for accurate *ab initio* descriptions of phonon-limited carrier mobilities should start from a proper treatment of these physical phenomena.

G. B., G.-M. R. and G. H. acknowledge financial support from F.R.S.-FNRS. H. P. C. M. acknowledges financial support from F.R.S.-FNRS through the PDR Grants HTBaSE (T.1071.15). M. G., M. J. V and

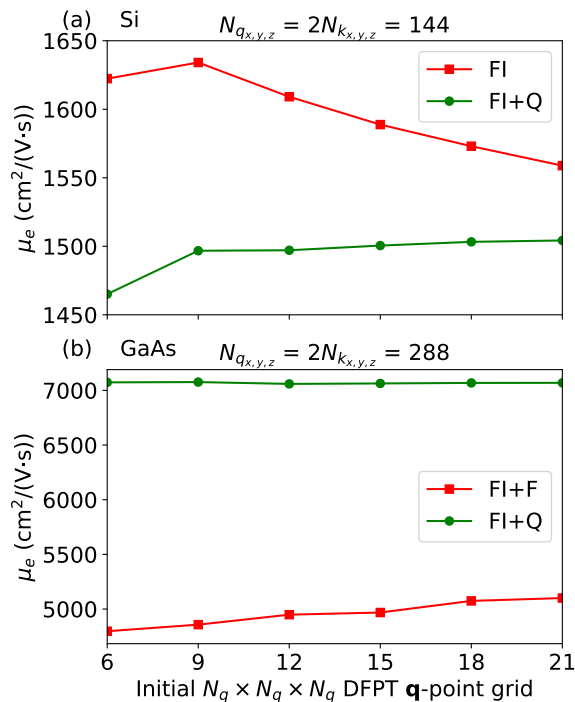


FIG. 3. Convergence of the electron mobility in (a) Si and (b) GaAs as a function of the initial DFPT \mathbf{q} -point grid. The linewidths and the mobilities are obtained by interpolating from these DFPT grids to (a) $72 \times 72 \times 72$ \mathbf{k} - and $144 \times 144 \times 144$ \mathbf{q} -point grids and (b) $144 \times 144 \times 144$ \mathbf{k} - and $288 \times 288 \times 288$ \mathbf{q} -point grids [18]. The red lines (FI and FI+F) include, for GaAs, the Fröhlich contribution only in the LR component of the potentials. The green line (FI+Q) includes both dipoles (for GaAs) and dynamical quadrupoles (Si and GaAs).

X. G. acknowledge financial support from F.R.S.-FNRS through the PDR Grants AIXPHO (T.0238.13) and ALPS (T.0103.19). M. J. V thanks FNRS and ULiege for a sabbatical grant in ICN2. M. S. and M. R. acknowledge the support of Ministerio de Economía, Industria y Competitividad (MINECO-Spain) through Grants No. MAT2016-77100-C2-2-P and No. SEV-2015-0496; of Generalitat de Catalunya (Grant No. 2017 SGR1506); and of the European Research Council (ERC) under the European Union’s Horizon 2020 research and innovation program (Grant Agreement No. 724529). The present research benefited from computational resources made available on the Tier-1 supercomputer of the Fédération Wallonie-Bruxelles, infrastructure funded by the Walloon Region under grant agreement n°1117545.

- [1] F. Giustino, *Rev. Mod. Phys.* **89**, 015003 (2017).
- [2] W. Kohn and L. Sham, *Phys. Rev.* **140**, A1133 (1965).
- [3] X. Gonze and C. Lee, *Phys. Rev. B* **55**, 10355 (1997).
- [4] S. Baroni, S. de Gironcoli, A. Dal Corso, and P. Gianozzi, *Rev. Mod. Phys.* **73**, 515 (2001).
- [5] F. Giustino, M. L. Cohen, and S. G. Louie, *Phys. Rev. B* **76**, 165108 (2007).
- [6] J. Sjakste, N. Vast, M. Calandra, and F. Mauri, *Phys. Rev. B* **92**, 054307 (2015).
- [7] S. Poncé, E. R. Margine, C. Verdi, and F. Giustino, *Comput. Phys. Commun.* **209**, 116 (2016).
- [8] L. A. Agapito and M. Bernardi, *Phys. Rev. B* **97**, 235146 (2018).
- [9] A. Eiguren and C. Ambrosch-Draxl, *Phys. Rev. B* **78**, 045124 (2008).
- [10] L. Chaput, A. Togo, and I. Tanaka, *Phys. Rev. B* **100**, 174304 (2019).
- [11] M. Born and K. Huang, *Dynamical theory of crystal lattices* (Clarendon press, 1954).
- [12] H. Fröhlich, *Adv. Phys.* **3**, 325 (1954).
- [13] C. Verdi and F. Giustino, *Phys. Rev. Lett.* **115**, 176401 (2015).
- [14] P. Vogl, *Phys. Rev. B* **13**, 694 (1976).
- [15] M. Royo and M. Stengel, *Phys. Rev. X* **9**, 021050 (2019).
- [16] M. Stengel, *Phys. Rev. B* **88**, 174106 (2013).
- [17] See Supplemental Material at <http://link> for more information about computational details and results.
- [18] G. Brunin, H. P. C. Miranda, M. Giantomassi, M. Royo, M. Stengel, M. J. Verstraete, X. Gonze, G.-M. Rignanese, and G. Hautier, *Unknown* **X**, XYZ (2020).
- [19] In order to simplify the notations, we replace $\partial_{\kappa\alpha,\mathbf{q}}v^{\text{KS}}(\mathbf{r})$ of Ref. [18] by $V_{\kappa\alpha,\mathbf{q}}(\mathbf{r})$.
- [20] X. Gonze, F. Jollet, F. A. Araujo, D. Adams, B. Amadon, T. Applencourt, C. Audouze, J.-M. Beuken, J. Bieder, A. Bokhanchuk, *et al.*, *Comput. Phys. Commun.* **205**, 106 (2016).
- [21] X. Gonze, B. Amadon, G. Antonius, F. Arnardi, L. Baguet, J.-M. Beuken, J. Bieder, F. Bottin, J. Bouchet, E. Bousquet, *et al.*, *Comput. Phys. Commun.* **248**, 107042 (2019).
- [22] We performed ground-state and DFPT phonon computations using norm-conserving pseudopotentials of the Troullier-Martins type [26], in the local-density approximation from Perdew and Wang [27] parametrized by Ceperley and Alder [28], with a plane-wave kinetic energy cutoff of 20 Ha for Si and 30 Ha for GaAs. The 3d semi-core states of Ga are not included in valence but this does not affect the conclusions of this work as we observed unphysical Gibbs oscillations also in calculations for GaP performed with GGA-PBE pseudopotentials including semi-core states. For phonon computations, the BZ is sampled using $18 \times 18 \times 18$ Γ -centered \mathbf{k} -point grids to obtain a good representation of the scattering potentials and a correct convergence of the Born effective charges, dielectric and quadrupolar tensors. We used different \mathbf{q} -meshes or \mathbf{q} -paths as explained in the text.
- [23] These results have been obtained with Quantum Espresso (QE) and EPW. We used the Perdew-Burke-Ernzerhof generalized-gradient approximation (GGA) for the exchange correlation functional and norm-conserving pseudopotentials from the PSEUDODOJO project [29, 30]. We

used an energy cutoff of 25 Ry for the plane-wave basis set and a lattice parameter of 5.47 Å. The matrix elements are interpolated starting from coarse Γ -centered $12 \times 12 \times 12$ \mathbf{k} -point and $6 \times 6 \times 6$ \mathbf{q} -point meshes. For the implementation of the quadrupolar corrections in EPW, we employed the quadrupole tensors computed by ABINIT as the same computation is not available in QE. Because of the different pseudopotentials, lattice parameters, and computational settings, we had to adjust the value of $\mathbf{Q}_{\kappa\alpha}$ to better describe the discontinuity, from 13.67 with LDA FHI [18] to 15.75 with GGA-PBE.

[24] G. K. H. Madsen, J. Carrete, and M. J. Verstraete, *Com-*

put. Phys. Commun. **231**, 140 (2018).

[25] S. Poncé, E. R. Margine, and F. Giustino, *Phys. Rev. B* **97**, 121201 (2018).

[26] N. Troullier and J. L. Martins, *Phys. Rev. B* **43**, 1993 (1991).

[27] J. P. Perdew and Y. Wang, *Phys. Rev. B* **45**, 13244 (1992).

[28] D. M. Ceperley and B. Alder, *Phys. Rev. Lett.* **45**, 566 (1980).

[29] M. J. Van Setten, M. Giantomassi, E. Bousquet, M. J. Verstraete, D. R. Hamann, X. Gonze, and G.-M. Rignanese, *Comput. Phys. Commun.* **226**, 39 (2018).

[30] D. R. Hamann, *Phys. Rev. B* **88**, 085117 (2013).

Electron-phonon beyond Fröhlich: dynamical quadrupoles in polar and covalent solids

Supplemental Material

Guillaume Brunin¹, Henrique Pereira Coutada Miranda¹, Matteo Giantomassi¹, Miquel Royo², Massimiliano Stengel^{2,3}, Matthieu J. Verstraete^{4,5}, Xavier Gonze^{1,6}, Gian-Marco Rignanese¹, and Geoffroy Hautier¹

¹*UCLouvain, Institute of Condensed Matter and Nanosciences (IMCN),
Chemin des Étoiles 8, B-1348 Louvain-la-Neuve, Belgium*

²*Institut de Ciència de Materials de Barcelona (ICMAB-CSIC),
Campus UAB, 08193 Bellaterra, Spain*

³*ICREA-Institució Catalana de Recerca i Estudis Avançats, 08010 Barcelona, Spain*

⁴*NanoMat/Q-Mat/CESAM, Université de Liège (B5), B-4000 Liège, Belgium*

⁵*Catalan Institute of Nanoscience and Nanotechnology (ICN2),
Campus UAB, 08193 Bellaterra, Spain and*

⁶*Skolkovo Institute of Science and Technology, Moscow, Russia*

(Dated: February 4, 2020)

I. CONTRIBUTION OF THE ELECTRIC-FIELD PERTURBATION TO THE LONG-RANGE POTENTIALS

In this section, we discuss the relative importance of the different terms in the LR model with particular emphasis on the effect associated to the response to the electric field \mathcal{E} . Figures S1–S4 show the average over the unit cell of the long-range model including different contributions: $V^{\mathcal{L}}$ includes Fröhlich, dynamical quadrupoles $\mathbf{Q}_{\kappa\alpha}$ and electric-field contributions, $V^{\mathcal{L}(F)}$ includes only the Fröhlich-like part, $V^{\mathcal{L}(F+Q)}$ includes all but the electric-field perturbation while $V^{\mathcal{L}(F+\mathcal{E})}$ includes all but the dynamical quadrupoles. The potentials are plotted along a \mathbf{q} -path, for a given atom (Ga, As, or Si) displaced along the first reduced direction (\hat{x}). The average of the model is compared to the average of the *exact* DFPT potentials obtained along the same \mathbf{q} -path. Comparing the different subplots produced with different models allows one to have a qualitative understanding of the importance of the

different terms and of their effect on the Fourier interpolation of the short-range part. More specifically, the plots show that the Fröhlich dipolar term alone is not able to capture the jump discontinuities around the Γ point, and that quadrupolar fields are necessary (in particular the term stemming from $\mathbf{Q}_{\kappa\alpha}$ as the contribution given by the electric-field perturbation is much smaller).

Figures S5–S8 show the average over the unit cell of the periodic part of the Fourier interpolated potentials including the same contributions as in Figs. S1–S4, and compared again to the *exact* DFPT potentials. These figures reveal that, without $\mathbf{Q}_{\kappa\alpha}$, the interpolated scattering potentials are affected by unphysical Gibbs oscillations around Γ because the discontinuity in \mathbf{q} -space is not removed when a model containing only the dipolar term is subtracted from the initial DFPT potentials before computing the Fourier transform.

As mentioned before, the term associated to \mathcal{E} plays a very minor role if we focus on the average of the potential over the unit cell that corresponds to the $\mathbf{G} = 0$ Fourier component. To appreciate the effect of the electric-field term, we need to focus on the \mathbf{q} -dependence of the Fourier components of the scattering potentials

$$\bar{V}_{\kappa\alpha,\mathbf{q}}(\mathbf{G}) = \frac{1}{\Omega} \int_{\Omega} d\mathbf{r} V_{\kappa\alpha,\mathbf{q}}(\mathbf{r}) e^{-i(\mathbf{q}+\mathbf{G})\cdot\mathbf{r}}, \quad (\text{S1})$$

for small $\mathbf{G} \neq 0$. In our tests we found that, for particular \mathbf{G} -vectors, the quantity in Eq. S1 as a function of \mathbf{q} presents (small) jump discontinuities for $\mathbf{q} \rightarrow 0$ and that the discontinuity is better described when the \mathcal{E} -term is included in the LR model. The results are summarized in Figs. S9 and S10. We performed the same analysis for GaP (not shown) and found very similar behavior. At the level of the mobility, the inclusion of the electric-field perturbation in the LR model changes the final results by 0.1% in GaAs and 0.01% in GaP when compared to calculations in which only dipoles and $\mathbf{Q}_{\kappa\alpha}$ are included. These results corroborate our affirmation done in the main text about the predominance of the dynamical quadrupoles over the electric field term in the case of GaAs and GaP.

II. EFFECT OF DYNAMICAL QUADRUPOLES ON THE INTERPOLATED PHONON DISPERSION

E-ph calculations are quite sensitive to the fine details of the electron and phonon dispersions. As discussed in more details in Ref. [15] of the main text, an expansion of the

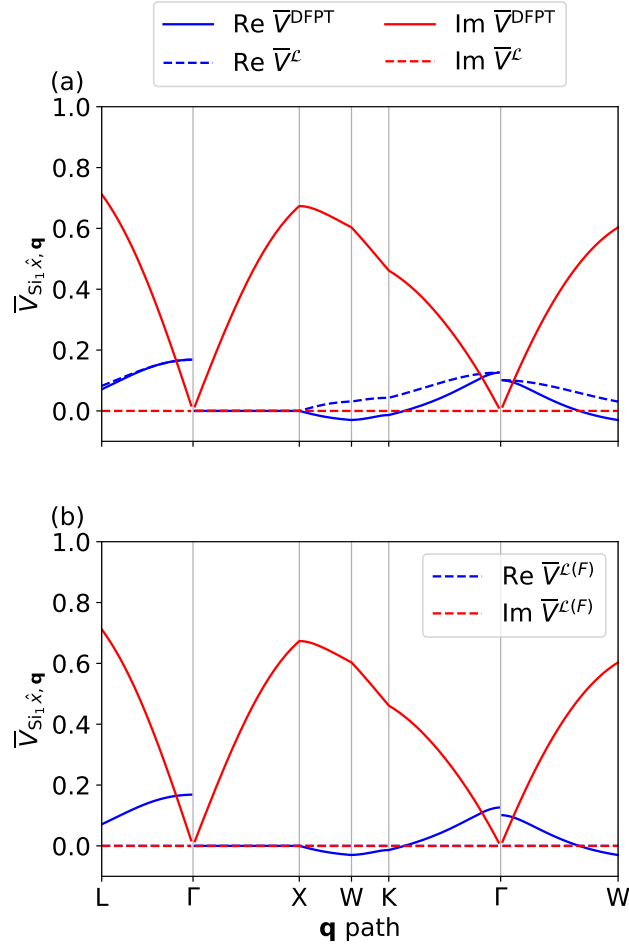


FIG. S1. (a) Average over the unit cell of the \hat{x} component of the DFPT (full lines) and long-range (dashed) e-ph potentials in Si, for the first atom located at (0,0,0). (b) Same as (a) but with the Fröhlich interaction only (equivalent to zero in Si).

dynamical matrix for $\mathbf{q} \rightarrow 0$ contains additional LR terms beyond the dipole-dipole interaction. These corrections are supposed to improve the quality and the stability of the Fourier interpolation of the phonon frequencies. It is therefore interesting to analyze the effect of the $\mathbf{Q}_{\kappa\alpha}$ on the convergence rate of the vibrational spectra for the three systems considered in this work.

Figure S11 shows the influence of the dipole-quadrupole and quadrupole-quadrupole interactions on the Fourier interpolation of the dynamical matrix in Si. The effects are small on the scale of the graph nevertheless the inclusion of these higher-order terms accelerates the convergence of the interpolation of the phonon spectrum with respect to the *ab initio* \mathbf{q} -grid. As mentioned in the main article, the effect on the mobility is estimated to be of

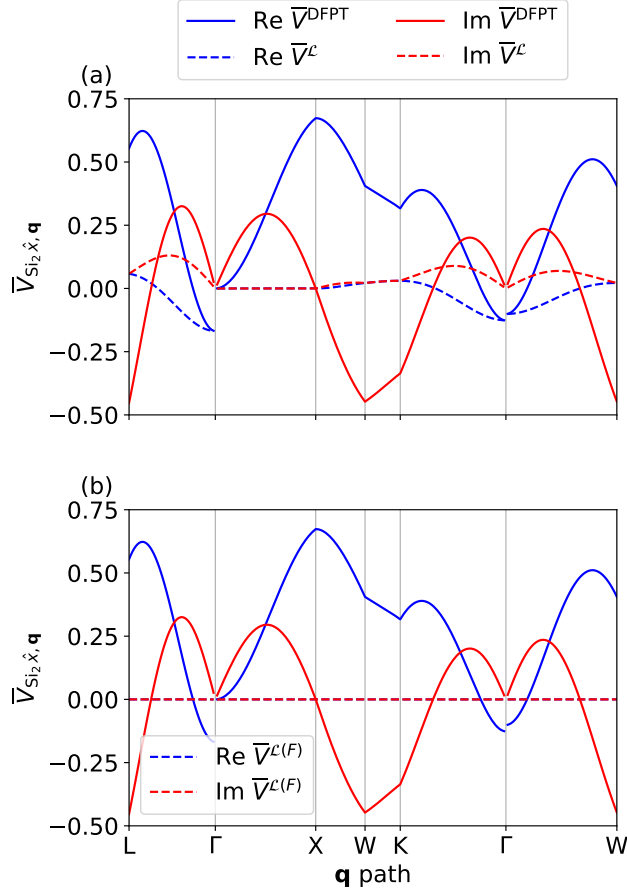


FIG. S2. (a) Average over the unit cell of the \hat{x} component of the DFPT (full lines) and long-range (dashed) e-ph potentials in Si, for the second atom located at $(1/4, 1/4, 1/4)$. (b) Same as (a) but with the Fröhlich interaction only (equivalent to zero in Si).

the order of 1%, value that is anyway larger than the one observed from the \mathcal{E} -term. We speculate that, in more “complicated” materials, the inclusion of these higher-order terms will play a more important role for the accurate description of the phonon dispersion in the long-wavelength limit. Figures S12 and S13 show the same comparison for GaP and GaAs.

III. CONVERGENCE OF THE MOBILITY IN GAP

Figure S14 shows the convergence of the electron mobility of GaP as a function of the initial *ab initio* \mathbf{q} -mesh. Similarly to what is observed in GaAs and Si, the inclusion of dynamical quadrupoles greatly accelerates the convergence with respect to the initial *ab*

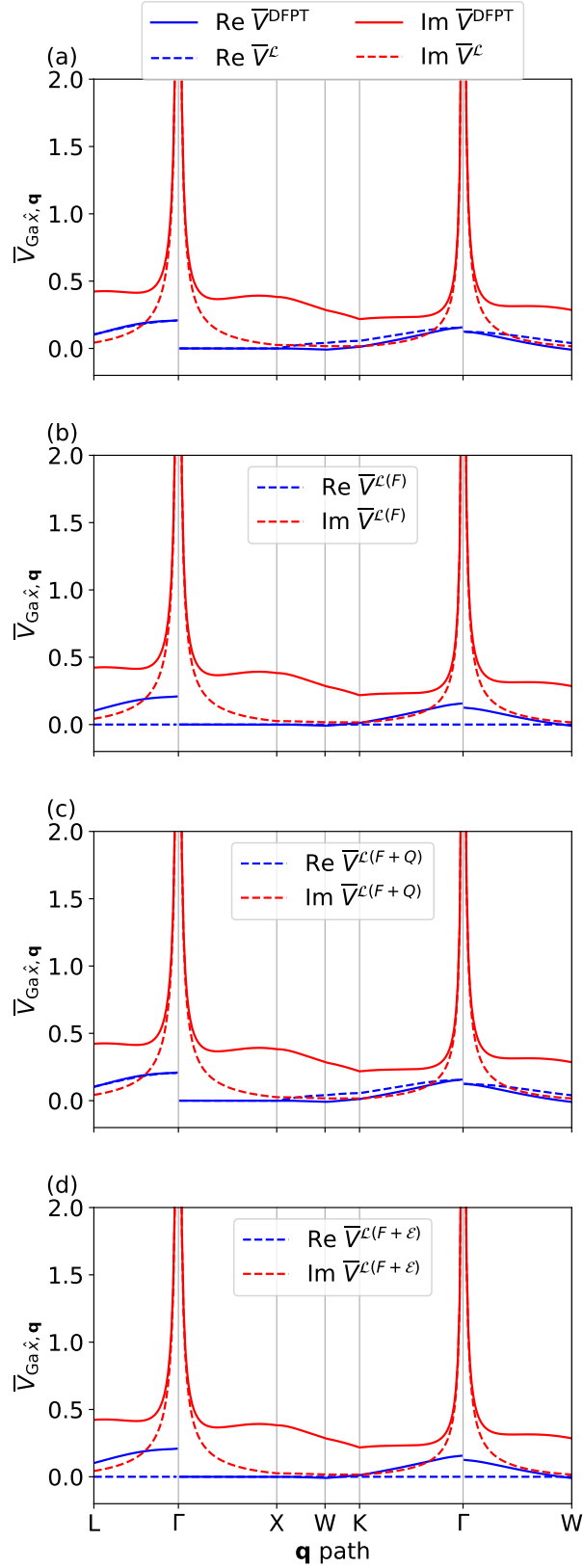


FIG. S3. (a) Average over the unit cell of the \hat{x} component of the DFPT (full lines) and long-range (dashed) e-ph potentials in GaAs for the Ga atom located at (0,0,0). (b), (c) and (d) show the decomposition of the different contributions to the long-range model.

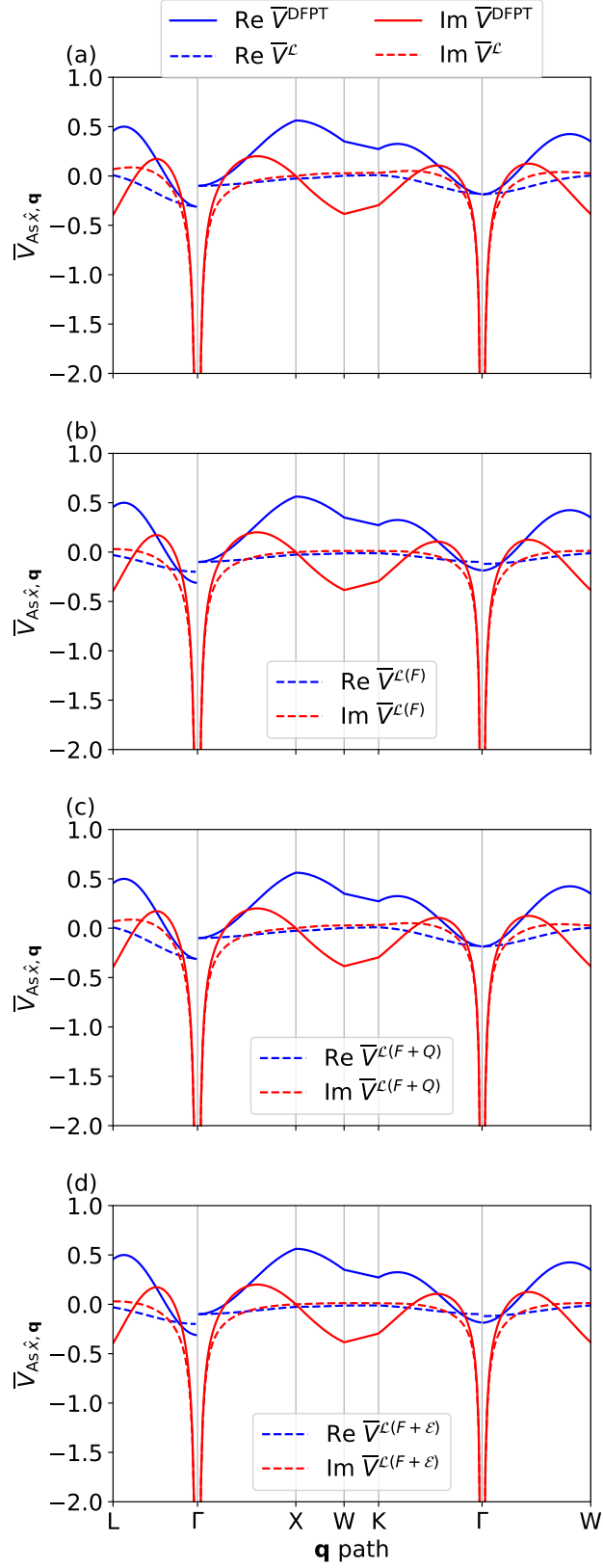


FIG. S4. (a) Average over the unit cell of the \hat{x} component of the DFPT (full lines) and long-range (dashed) e-ph potentials in GaAs, for the As atom located at $(1/4, 1/4, 1/4)$. (b), (c) and (d) show the decomposition of the different contributions to the long-range model.

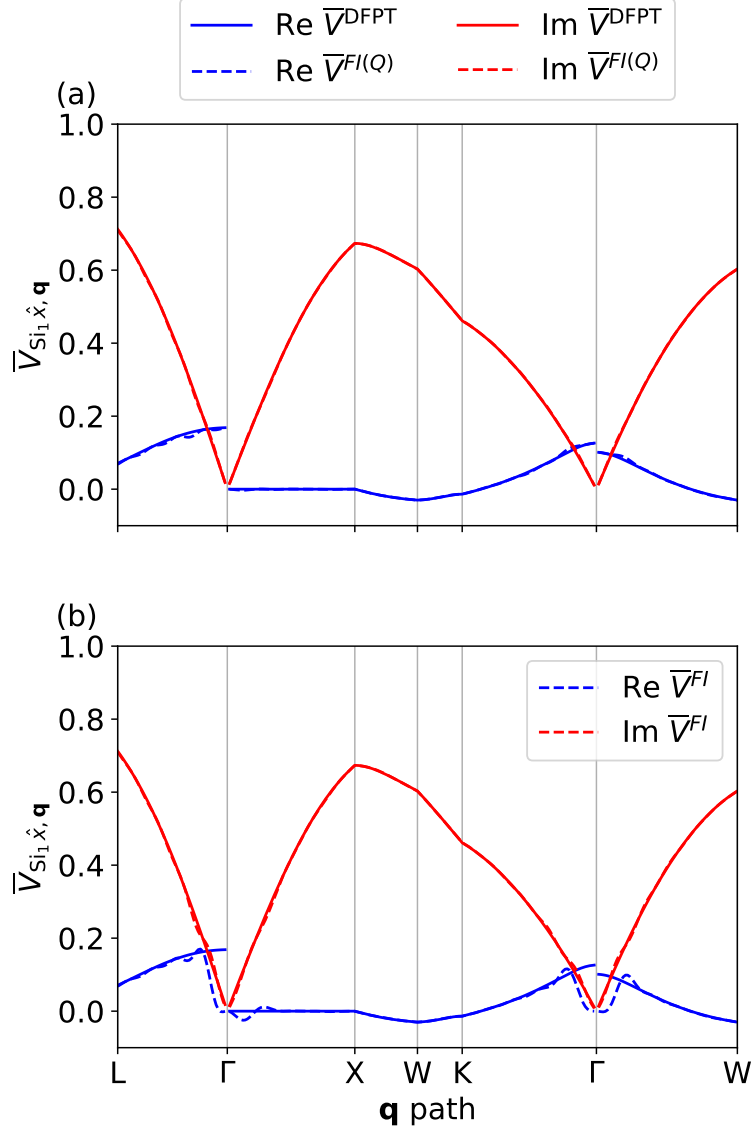


FIG. S5. (a) Average over of the unit cell of the \hat{x} component of the DFPT (full lines) and Fourier-interpolated (dashed) e-ph potentials in Si, for the first Si atom located at (0,0,0). (b) Same as (a) but with the Fröhlich interaction only (equivalent to zero in Si).

initio \mathbf{q} -mesh.

IV. IMPORTANCE OF THE REGION AROUND Γ

Figures S15 and S16 show the number of \mathbf{q} -points included in the computation of the imaginary part of the e-ph self-energy and the sum of the absolute value of the e-ph matrix elements as a function of the length of the \mathbf{q} -point. An important fraction of phonon-

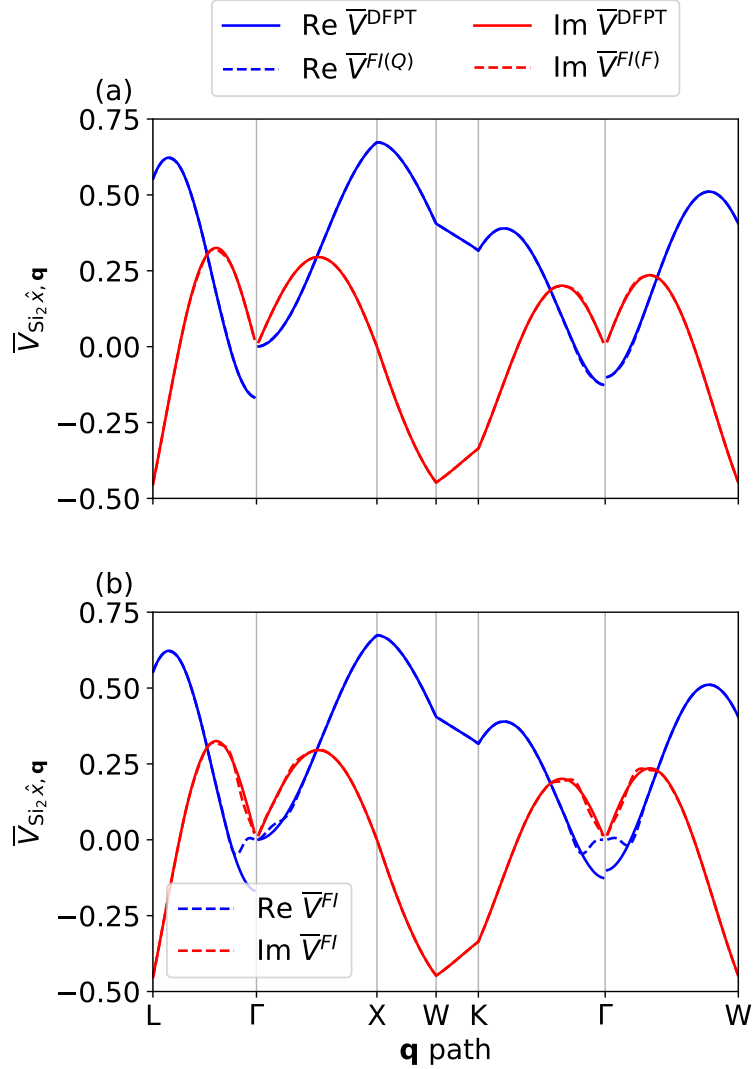


FIG. S6. (a) Average over the unit cell of the \hat{x} component of the DFPT (full lines) and Fourier-interpolated (dashed) e-ph potentials in Si, for the second atom located at $(1/4, 1/4, 1/4)$. (b) Same as (a) but with the Fröhlich interaction only (equivalent to zero in Si).

mediated transitions involve small momentum transfer with significant probability amplitude. In GaAs (Fig. S16) the e-ph matrix elements show a sudden increase for small $|\mathbf{q}|$ because of the Fröhlich divergence. Note that the analysis of the e-ph matrix elements takes into account crystal momentum conservation but not energy conservation in the sense that all the phonon modes ν are included in the sum of the absolute value of the e-ph matrix elements.

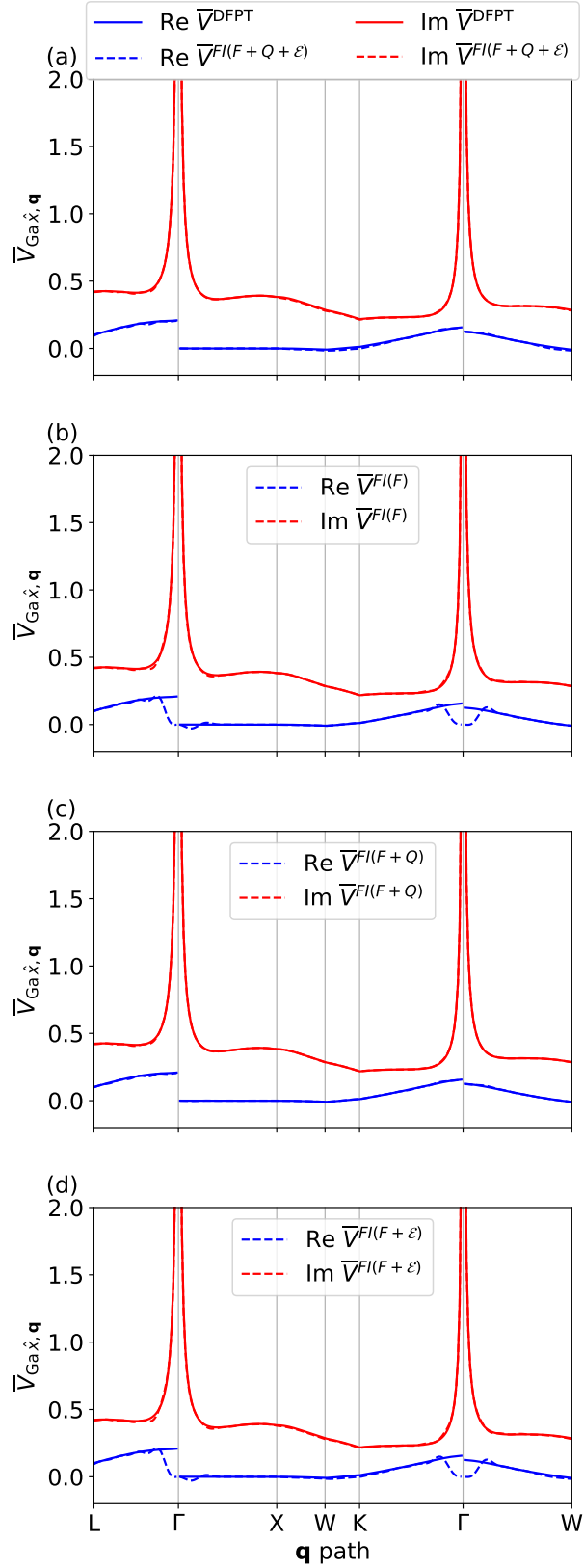


FIG. S7. (a) Average over the unit cell of the \hat{x} component of the DFPT (full lines) and Fourier-interpolated (dashed) e-ph potentials in GaAs for the Ga atom located at (0,0,0). (b), (c) and (d) show the decomposition of the different contributions to the long-range model.

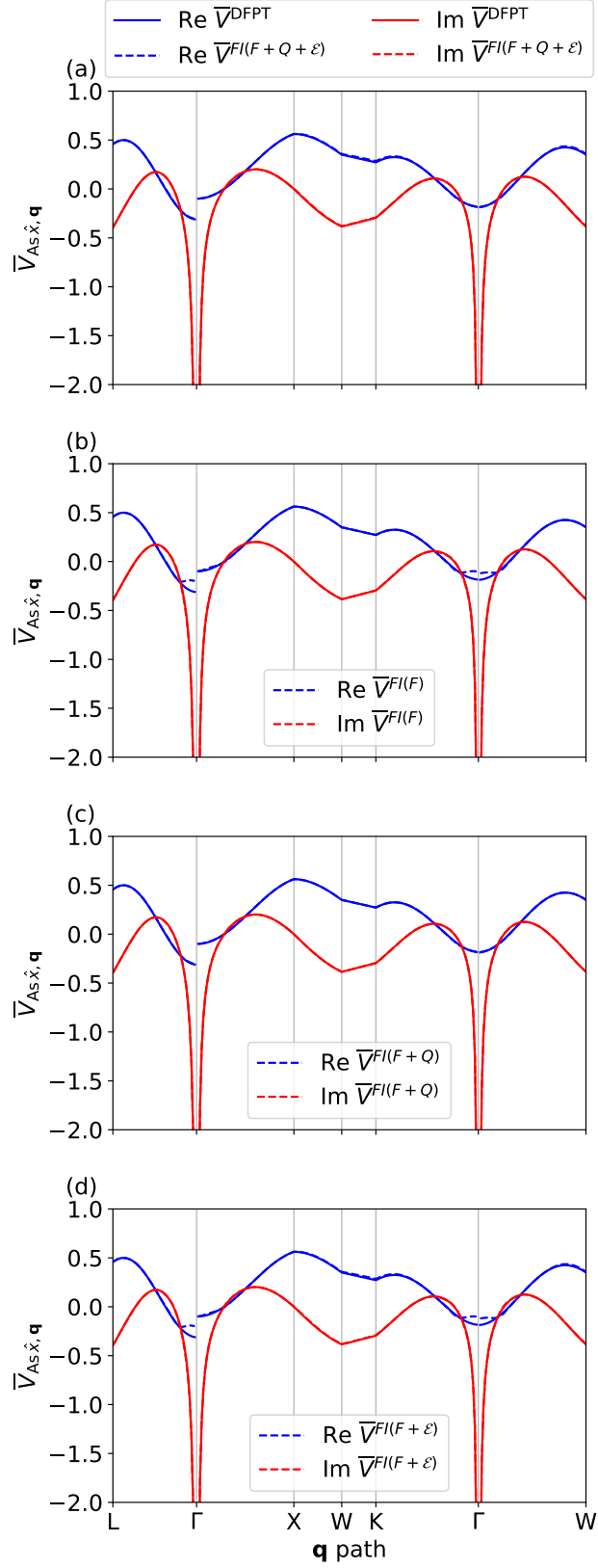


FIG. S8. (a) Average over the unit cell of the \hat{x} component of the DFPT (full lines) and Fourier-interpolated (dashed) e-ph potentials in GaAs, for the As atom located at $(1/4, 1/4, 1/4)$. (b), (c) and (d) show the decomposition of the different contributions to the long-range model.

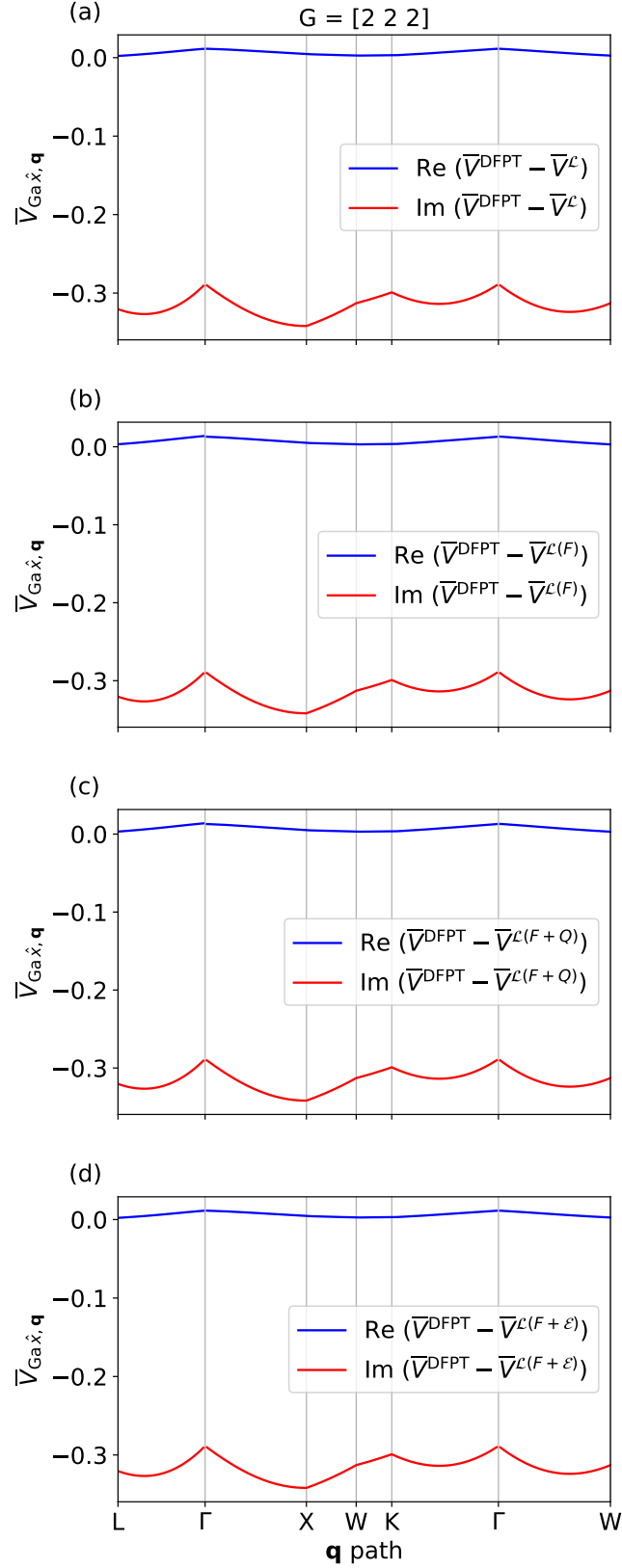


FIG. S9. (a) Fourier component of the \hat{x} component of the DFPT (full lines) and long-range (dashed) e-ph potentials in GaAs, for the Ga atom located at (0,0,0). (b), (c) and (d) show the decomposition of the different contributions to the long-range model. Only a specific \mathbf{G} component of the potential is shown.

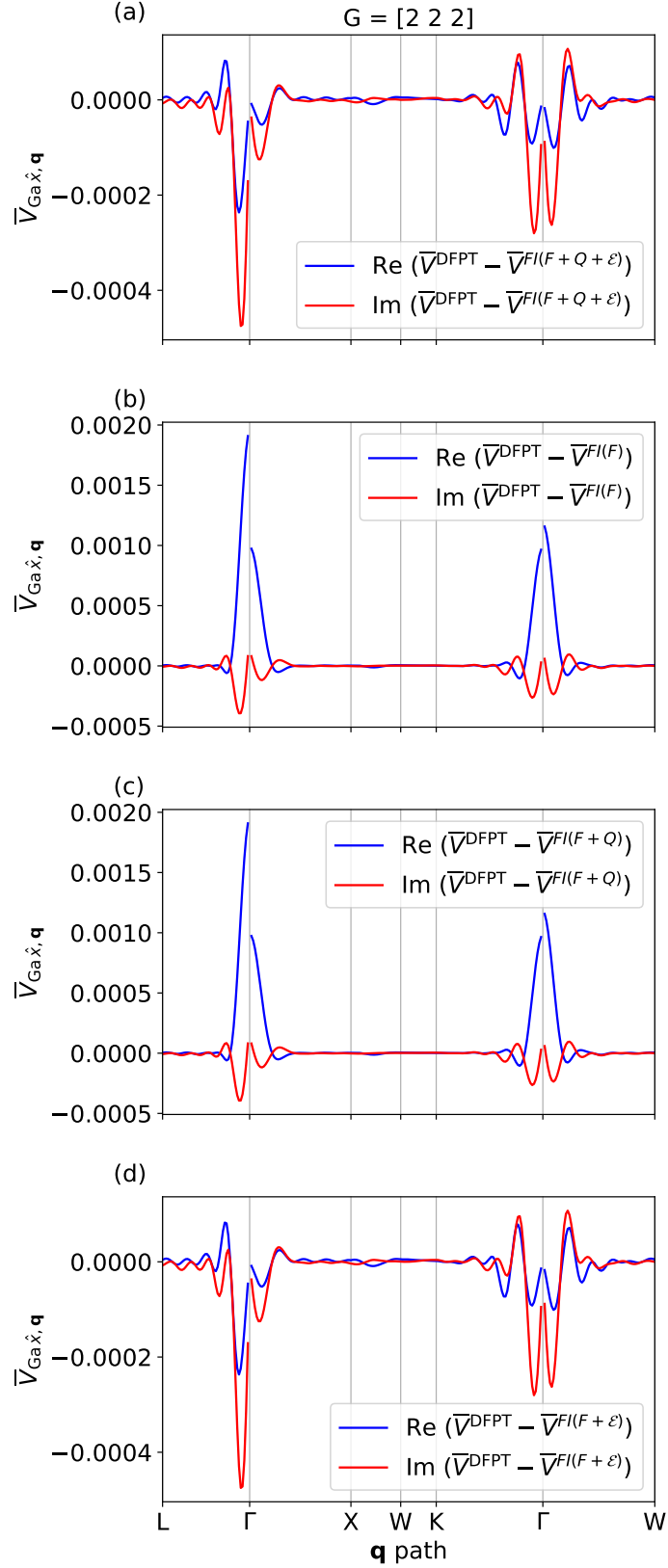


FIG. S10. (a) Fourier component of the \hat{x} component of the DFPT (full lines) and Fourier-interpolated (dashed) e-ph potentials in GaAs, for the Ga atom located at (0,0,0). (b), (c) and (d) show the decomposition of the different contributions to the long-range model. Only a specific \mathbf{G} component of the potential is shown.

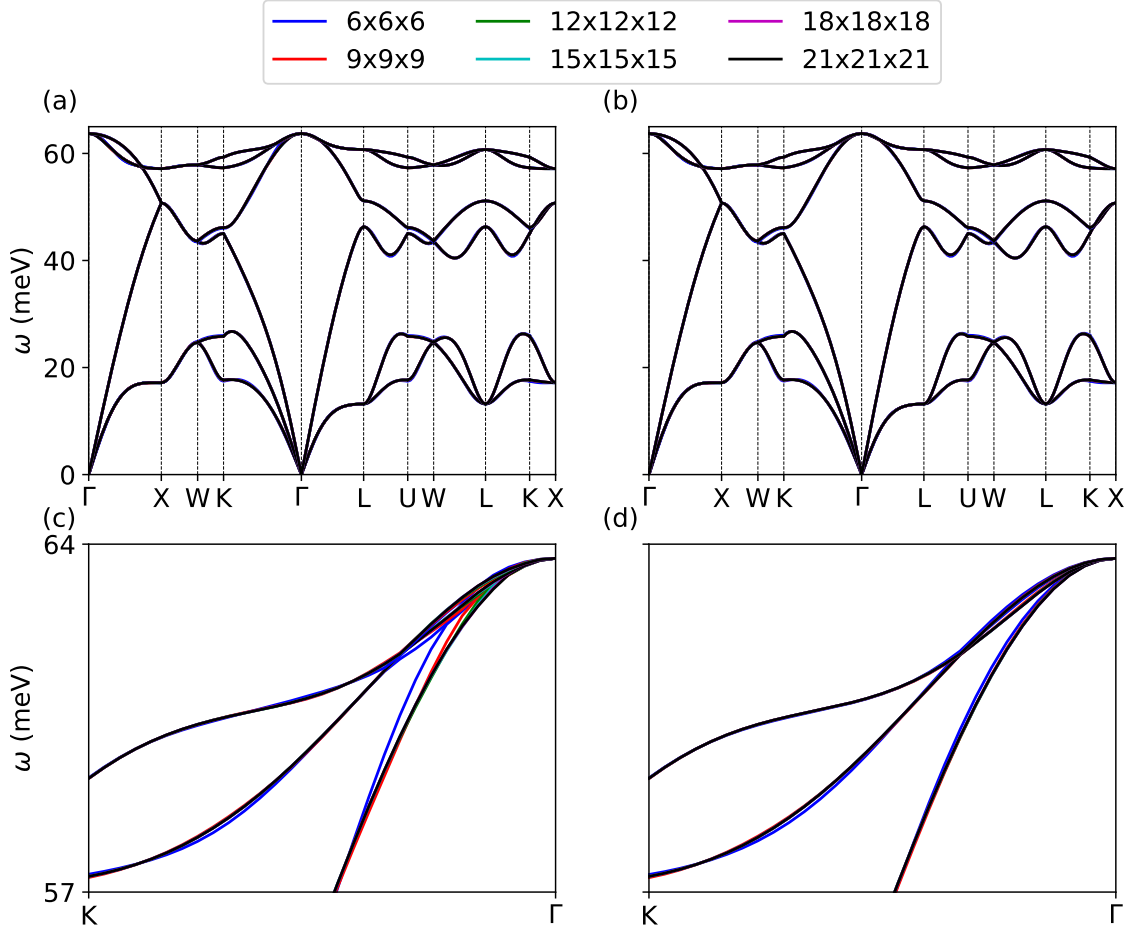


FIG. S11. Phonon dispersion in Si without (a) and with (b) the inclusion of dipole-quadrupole and quadrupole-quadrupole interactions in the Fourier interpolation of the dynamical matrix. (c), (d) Zoom over the regions in (a), (b) containing the most important changes.

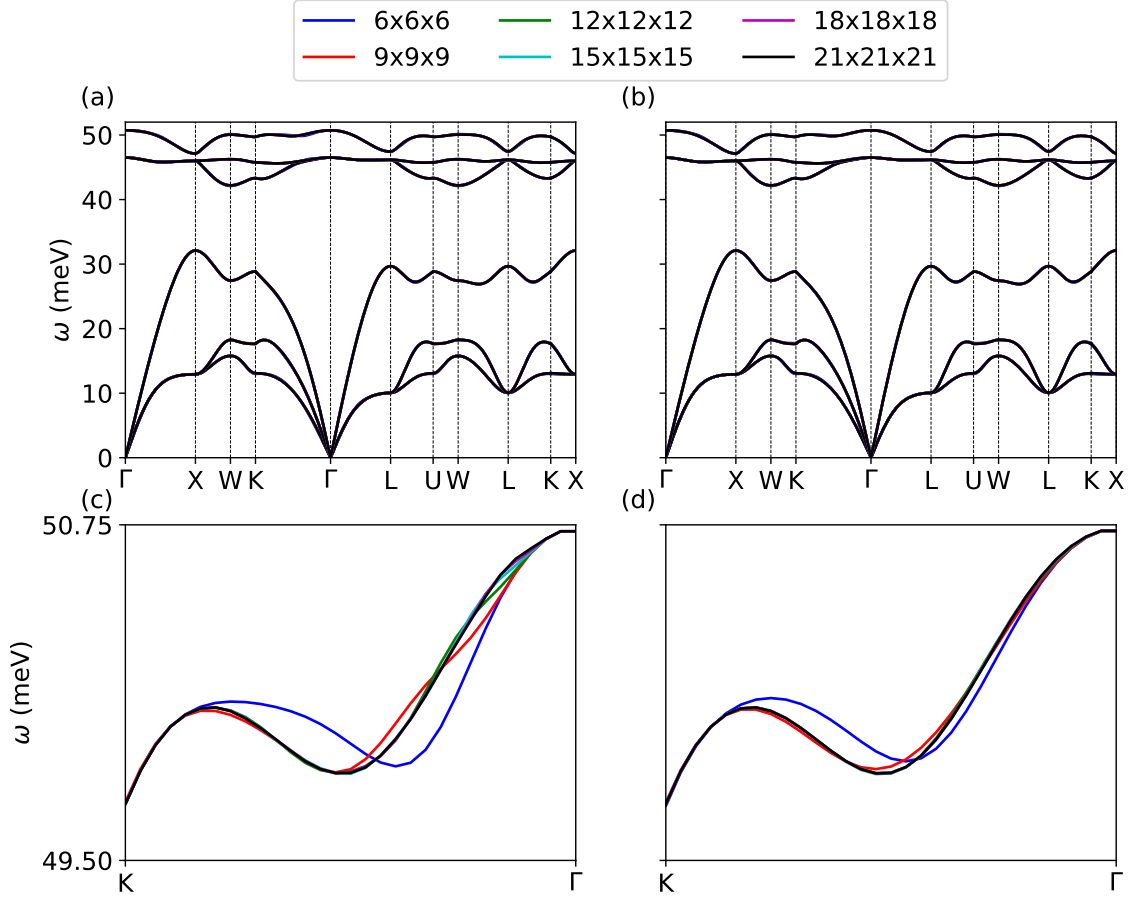


FIG. S12. Phonon dispersion in GaP without (a) and with (b) the inclusion of dipole-quadrupole and quadrupole-quadrupole interactions in the Fourier interpolation of the dynamical matrix. (c), (d) Zooms over the regions in (a), (b) containing the most important changes.

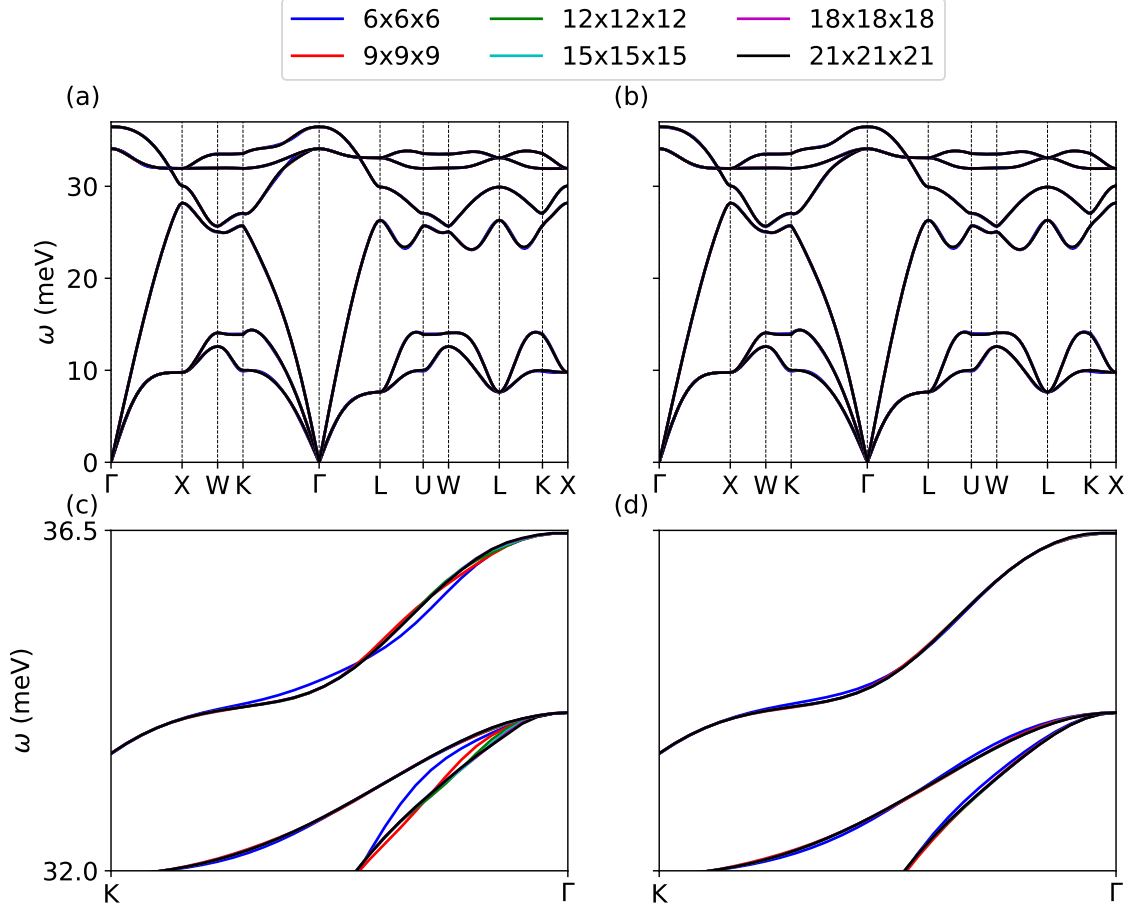


FIG. S13. Phonon dispersion in GaAs without (a) and with (b) the inclusion of dipole-quadrupole and quadrupole-quadrupole interactions in the Fourier interpolation of the dynamical matrix. (c), (d) Zoom over the regions in (a), (b) containing the most important changes.

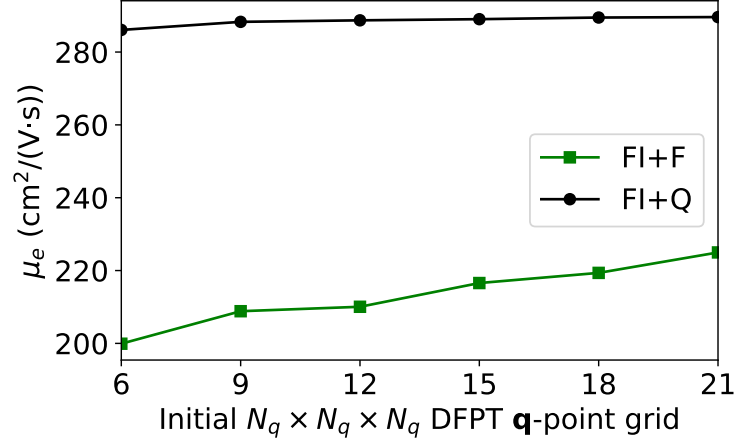


FIG. S14. Convergence of the electron mobility in GaP as a function of the initial DFPT \mathbf{q} -grid. The linewidths and the mobilities are obtained by interpolating from these initial DFPT grids to $78 \times 78 \times 78$ \mathbf{k} - and $156 \times 156 \times 156$ \mathbf{q} -point grids. The green curve includes the Fröhlich term only in the LR model whereas the black curve includes both dipoles and dynamical quadrupoles.

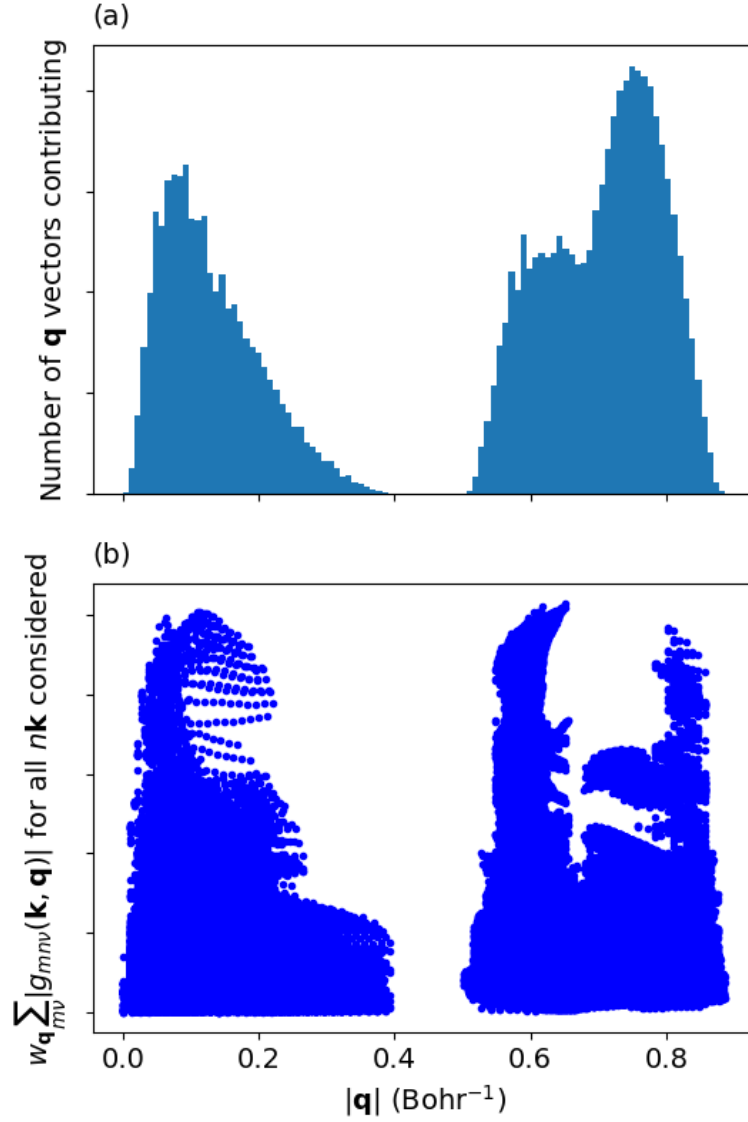


FIG. S15. (a) Distribution of the number of \mathbf{q} -points used in the integration of the electron lifetimes in Si as a function of $|\mathbf{q}|$. (b) Values of the e-ph matrix elements $g_{mn\nu}(\mathbf{k}, \mathbf{q})$ summed over m and ν , for all the $n\mathbf{k}$ states considered relevant for the computation of the mobility. The weight of the \mathbf{q} -points are also taken into account. This figure reveals that the sampling of the region around Γ significantly contributes to the final results.

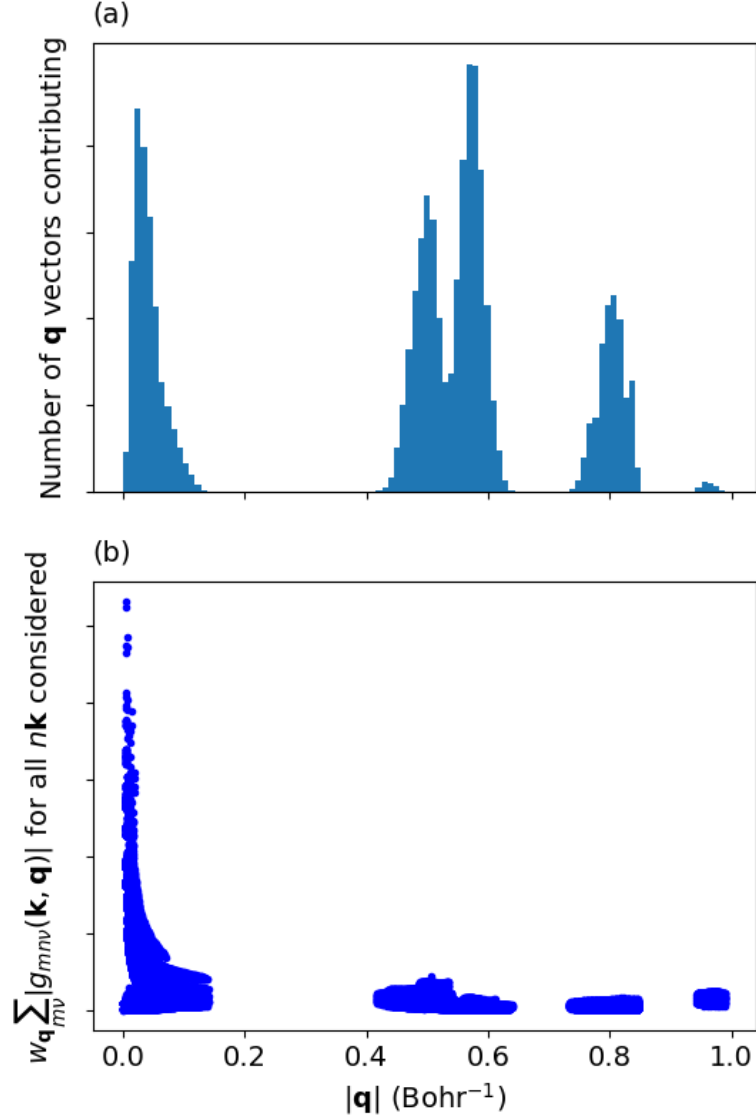


FIG. S16. (a) Distribution of the number of \mathbf{q} -points used in the integration of the electron lifetimes in GaAs as a function of $|\mathbf{q}|$. (b) Values of the e-ph matrix elements $g_{mn\nu}(\mathbf{k}, \mathbf{q})$ summed over m and ν , for all the $n\mathbf{k}$ states relevant for the computation of the mobility. The weight of the \mathbf{q} -point is also taken into account. These show that the the sampling of the region around Γ is very important.